Development and Validation of a Simple Antigen–Antibody Model

N. A. Busch, Y. C. Chiew, and M. L. Yarmush
Dept. of Chemical and Biochemical Engineering, Rutgers University, Piscataway, NJ 08854

M. S. Wertheim
Dept. of Physics, Michigan Technological University, Houghton, MI 49931

A theoretical model for investigating physical phenomena underlying immune complex formation was developed, based on the statistical mechanical theory of associating fluids that identifies each molecule as a hard sphere with a nested point charge and vector dipole. The interaction between binding molecules (epitope–paratope binding) is represented as a cone truncated by two concentric spheres in which the potential energy is a modified square well with respect to particle separation and a square well with respect to mutual molecular orientation. Equilibrium binding results predicted by the model show good agreement with results obtained experimentally for a model system containing a single antigen and a single monoclonal antibody [bovine serum albumin (BSA)–anti-BSA antibody]. Moreover, values obtained for the system isothermal compressibility and the second virial coefficient by both the model and light scattering experiments also show good agreement with one another.

Introduction

Immune complexes are formed by the reversible, noncovalent bonding of antigens and antibodies. Antibodies are bivalent proteins, produced by the immune system, that can associate with both soluble and particulate foreign substances called *antigens*. The formation of immune complexes is an essential step in the process by which the antigens are removed from the immune system. The rate at which soluble immune complexes are cleared by the reticuloendothelial system (Paul, 1986) depends in part on the size and shape distribution of these immune complexes (Garred et al., 1989, 1990; Segal et al., 1983; Weiss et al., 1990).

In previous work using electron-microscopic and dynamic light-scattering techniques our laboratory has shown that the size and shape of immune complexes can be quite polydisperse even when monodisperse antigen and antibody molecules are used (Murphy, 1989; Murphy et al., 1988). It was observed that certain combinations of antibodies, which bind noncompetitively to a model antigen, produced predominately long chain immune complexes, while another combination yielded a large number of small cyclic complexes. Although a phenomenological model was developed to provide insight into these observations (Murphy et al., 1990), a deeper understanding based upon some foundation of intermolecular interactions was lacking.

In the present article we develop a simplified statistical mechanical model, based on the theory of associating fluids, that can be used to investigate several parameters that are important in determining the complex shape and size distributions: short-ranged interactions that contribute to the equilibrium association constant, or affinity; steric hindrance to binding due to epitope location; and center-to-center interactions. In the present study we have begun this analysis by validating the model through comparison of equilibrium binding results obtained from our model with those obtained by radioimmunoassay experiments. In addition we show that the isothermal compressibility and static structure functions predicted by the model compare well with values obtained from independent light-scattering experiments.

Materials and Methods

Bovine serum albumin

Bovine serum albumin (BSA) (Pentex monomer standard, Miles Laboratories, Elkhardt, IN) was dissolved in phos-

Correspondence concerning this article should be addressed to M. L. Yarmush.

phate-buffered saline (PBSA: 0.15 $\mathfrak{M}$ NaCl, 0.01 $\mathfrak{M}$ KH_2PO_4, 0.01 $\mathfrak{M}$ K_2HPO_4, pH 7.0) with 0.02% (w/v) sodium azide, purified by gel permeation chromatography on a Sephadex G-150 (Pharmacia Fine Chemicals, Piscataway, NJ) column, and concentrated in a stirred ultrafiltration cell with a YM-10 membrane (Amicon, Danvers, MA). BSA monomer homogeneity was checked by high-performance liquid chromatography (HPLC) and dynamic light scattering (DLS) (BI-200 SM, Brookhaven Instruments Corporation, Holtsville, NY). The effective charge on BSA was determined by titration measurements (Tanford, 1952, 1955; Tanford et al., 1955). BSA concentration was determined by measuring the optical density at 280 nm and using a standard measured extinction coefficient of 0.66 mg/ml·cm. Stock solutions of ~ 6–7 mg/mL were stored at 4.0°C.

Monoclonal antibodies

The anti-BSA monoclonal antibodies (MAb) have been characterized in detail in regards to their association constant, subclass, and BSA subdomain specificity (Morel et al., 1988). The MAb were selected in combinations such that they bind noncompetitively to three separate BSA subdomains. The three monoclonal antibodies ($Ab_{5.1}$, $Ab_{6.1}$, and $Ab_{9.1}$) were purified by affinity chromatography from ascites fluid according to standard laboratory protocols (Morel et al., 1988). The antibodies were characterized using dynamic light scattering, sodium dodecyl sulfate–polyacrylamide gel electrophoresis (SDS-PAGE) and isoelectric focusing (IEF). The stock solution concentrations ranged from 1 to 3 mg/mL (0.65×10^{-5} to 5.2×10^{-5} $\mathfrak{M}$) and were stored at 4°C. Concentration is determined by optical density measurement at 280 nm using standard measured extinction coefficients (such as 1.5, 1.45, and 1.7 mg/mL·cm for $Ab_{5.1}$, $Ab_{6.1}$, and $Ab_{9.1}$, respectively). The charge on the antibodies was determined by titration measurements (Tanford, 1955). Monomer antibody homogeneity was checked with HPLC using a TSK 3000 column before use.

Light scattering

The dynamic light-scattering measurements are carried out on using a Brookhaven goniometer (BI-200 SM, Brookhaven Instruments Corporation, Holtsville, NY). The photon autocorrelation function (Berne and Pecora, 1975) was measured by a correlator (BI-2030-AT, Brookhaven Instrument Corporation, Holtsville, NY) and recorded for analysis by an IBM PC/AT microcomputer. The laser (Stabilite 2016-4, Spectra Physics, Mountain View, CA) and goniometer are mounted on a Newport 500-k optical instrument table. The index matching fluid and sample cell are maintained at constant temperature, ±0.1°C, by continuously circulating water from a water bath (Model RC-6, Brinkmann Instruments Corp., Westbury, NY).

The diffusion coefficient of each protein in this study was determined from dynamic light-scattering measurements according to standard laboratory protocol (Murphy et al., 1988). The static structure function was determined as follows: The photon intensity autocorrelation function was analyzed to obtain the first-order correlation function (Provencher, 1979) $g_E^{(1)}(t, q)$. The first cumulant μ_1 was computed as

$$\mu_1 = -\lim_{t\to 0}\left\{\frac{\partial}{\partial t}\ln(g_E^{(1)}(t, q))\right\}. \quad (1)$$

For a system of noninteracting molecules, each with molecular weight m_i and number density N_i, the first-order autocorrelation function can be written as (Ackerson, 1976)

$$g_E^{(1)}(t, q) = \sum_i \mathcal{G}_i(q)\exp(-\Gamma_i(q)t). \quad (2)$$

The wave number is $q = (4\pi n/\lambda)\sin(\theta/2)$ and the solvent index of refraction at wavelength λ is n. The scattering angle is θ. The Lorenzian linewidth for each species is $\Gamma_i(q) = q^2\mathfrak{D}_i$ and $\mathfrak{D}_i$ is the dilute limit diffusion coefficient. The Lorenzian weight is $\mathcal{G}_i = N_i m_i^2\mathfrak{D}_i/\Sigma_i N_i m_i^2$. The mean linewidth $\bar{\Gamma}_{90}$ for the system of noninteracting molecules is computed using Eq. 2 to yield the static structure function as $S(q) = \bar{\Gamma}_{90}/\mu_1$. Since the static structure function for the single-component protein systems used in this study are unity for all scattering angles, the measured total structure function that is different from unity is due to the antigen–antibody complex.

Model Development

To study the physical phenomena that influence the complex size and shape distributions we have developed a model system of BSA as our model antigen and three IgG1 anti-BSA antibodies ($Ab_{5.1}$, $Ab_{6.1}$, $Ab_{9.1}$). BSA is a prolate ellipsoid protein of molecular weight 66.2 kDa, major axis 141 Å, and minor axis 40 Å. $Ab_{5.1}$ binds to the carboxyl region of domain I, $Ab_{6.1}$ binds to the amino region of domain I, and $Ab_{9.1}$ binds to the carboxyl region of III (Morel et al., 1988) as shown in panel (a) of Figure 1. The charges on domains I, II, and III are $-10.0e^-$, $-8.0e^-$, and $+0.0e^-$, respectively (Peters, 1985). The dipole moment for the BSA and the antibody molecules is indicated in Figure 1.

The anti-BSA antibodies, shown in panel (b) of Figure 1, are IgG1 κ1 immunoglobulins composed of two heavy chain and two light chain polypeptides. The two heavy chains are disulfide cross-linked to form the F_c unit. One light chain is bound to a heavy chain polypeptide to form each F_{ab} unit. The paratope that binds to a specific region on the antigen called an *epitope* is located at the end of each F_{ab} unit. The distance between the paratopes corresponds to an angle of ~ 90 to ~ 160° of arc between the F_{ab} units. In the antibodies used here, the F_{ab} units are positively charged and the F_c is negatively charged; the dipole moment is presumed to be oriented from the F_c unit and bisect the angle between the F_{ab} units.

The epitope–paratope interaction occurs between complementary surfaces (Amit et al., 1986) as shown in Figure 2. The forces responsible for the antigen–antibody bond are due to hydrogen bonding between the two surfaces, electrostatic and hydrophobic interactions (Pauling, 1940), and yield a contribution to the overall intermolecular potential as indicated by Φ^{ss} in Figure 2. The bonding interaction between the epitope and paratope depends upon the relative orientation of the antigen and antibody (Padlan et al., 1990) and upon the separation between the surfaces (Tulip et al., 1989). The center-to-center electrostatic forces, as indicated by Φ^{cc} in Figure 2, contribute to the overall intermolecular potential energy.

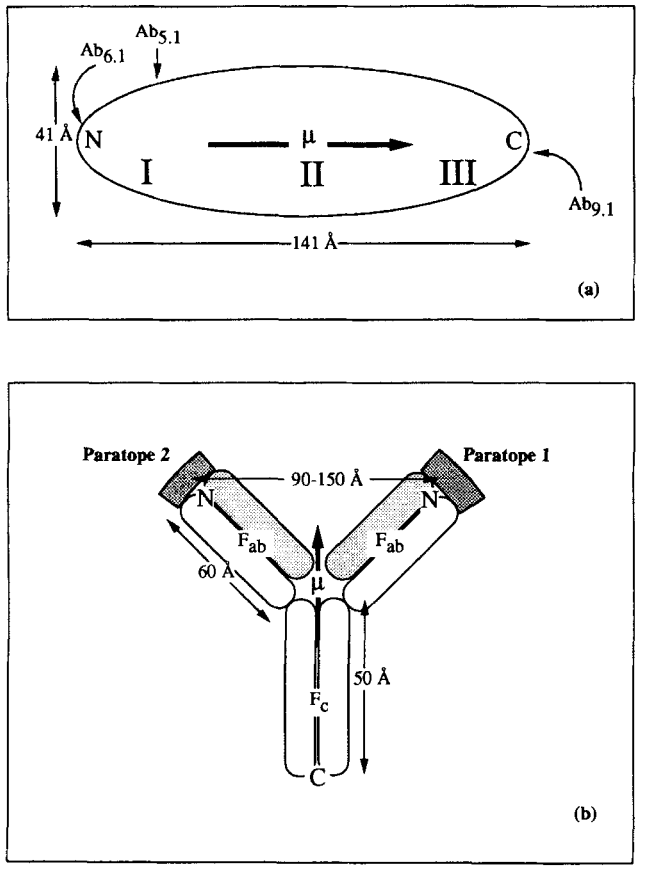

Figure 1. (a) BSA and (b) a type IgG anti-BSA antibody.

BSA is a prolate ellipsoid molecule with major axis length 141 Å, minor axis 40 Å, hydrodynamic radius in 0.15 M PBS-A of 35.0 Å, and molecular weight 66.2 kDa. BSA is composed of three charged domains, (I, II, and III), and has a pI of 4.9–5.1. $Ab_{5.1}$ binds to I-C, $Ab_{6.1}$ binds to I-N, and $Ab_{9.1}$ binds to III-C. The anti-BSA antibody, shown in panel (b), has a 57.0 Å hydrodynamic radius, and a 155.0 kDa molecular weight. The antibodies, $Ab_{5.1}$, $Ab_{6.1}$, and $Ab_{9.1}$, are positively charged at neutral pH.

Including all physical details of the BSA and antibodies in the model is prohibitive in terms of computational expense. We propose that the two major influences on the complex distributions are the epitope–paratope and center-to-center potential energies. The center-to-center potential is assumed to consist of a spherically symmetric charge–charge potential and a point dipole moment at the center of each molecule. The van der Waals interaction is ignored as it is weaker than the electrostatic interactions of interest (Buckingham and Popel, 1955a, 1955b). Temporal effects, such as hydrodynamic interactions, are not included in this model.

Since this model is being developed to permit investigation of systems composed of two antibodies against BSA, two epitopes are included on BSA. The center of each paratope is represented by the vector $\mathbf{r}_{js}$, $s = A, B$. The angle between the paratopes on each antibody is Ψ_{Ab} as shown in Figure 3. The center of each epitope has the vector representation $\mathbf{r}_{is}$, $s = A, B$. The epitope locations on the BSA are unknown, so their relative position is a variable for study. The angle between the epitopes is Ψ_{Ag}. The orientation of the spherical protein model is determined by the dipole moment, therefore

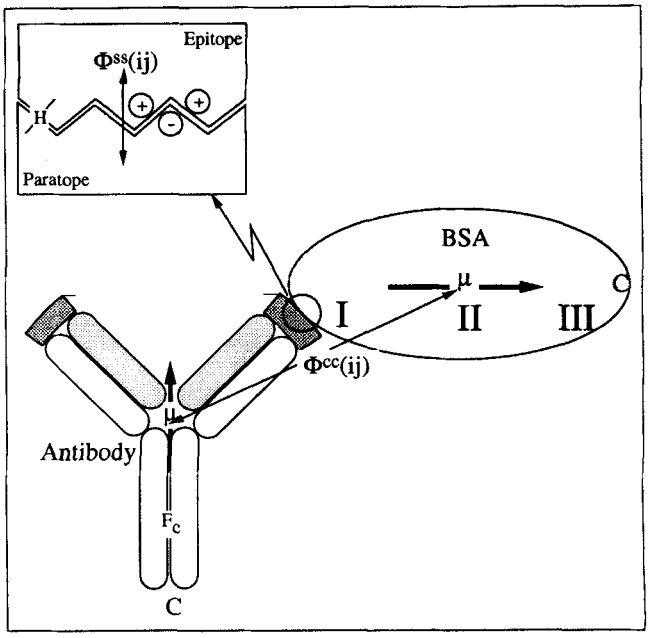

Figure 2. BSA and α-BSA antibody center-to-center interaction as well as the paratope–epitope interaction.

The α-BSA interaction is binding to BSA in the I-N position. The paratope–epitope bonding energy may include both hydrogen bonding energies (indicated by the capital H) and charge–charge energies.

both Ψ_{Ab} and Ψ_{Ag} as well as $\mathbf{r}_{is}$ and $\mathbf{r}_{js}$ correspond to unique and well-determined locations for the binding sites (see Figure 3).

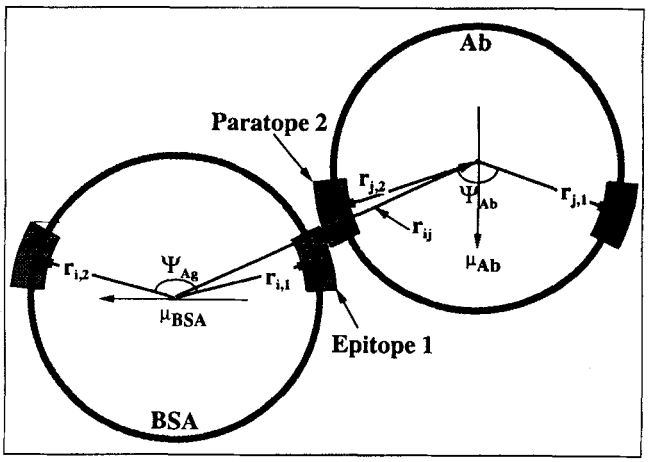

Figure 3. Model of BSA and type IgG anti-BSA antibody showing the Ab–BSA bond (not drawn to scale).

The antibody and BSA are represented by the shaded spots where the paratopes and epitopes are indicated. In this case, epitope A, defined by the vector $\mathbf{r}_{is} = \mathbf{r}_{iA}$, is bonded to paratope B, defined by the vector $\mathbf{r}_{js} = \mathbf{r}_{jB}$. The angle between the vectors defining the two epitopes on BSA, $\mathbf{r}_{iA}$ and $\mathbf{r}_{iB}$, is Ψ_{Ag}. The corresponding angle between the paratopes on the antibody is Ψ_{Ag}. For BSA and the antibody to be bonded, the vector from the center of BSA to the center of the antibody, $\mathbf{r}_{ij}$, must pass through both the epitope and paratope.

Intermolecular Potential

The total number density for the system composed of BSA and a single antibody is ρ. We employ the lowercase i as an index for the BSA molecules and j as an index for the antibody molecules. The uppercase indices A and B refer to the binding sites on either BSA or the antibody. Site A of particle i is denoted $[i, A]$. The charge, the dipole moment magnitude, the number fraction, orientation, and the position of the center of particle i are Z_i, μ_i, $X^{(i)}$, Ω_i, and $\mathbf{r}_i$, respectively. The mutual position and orientation of i and j (that is, $(\mathbf{r}_i, \Omega_i, \mathbf{r}_j, \Omega_j)$) is denoted (ij). The center-to-center vector from particle i to particle j is $\mathbf{r}_{ij} = \mathbf{r}_j - \mathbf{r}_i$ with magnitude $r_{ij} = |\mathbf{r}_{ij}|$; the corresponding unit vector is $\mathbf{u}_{ij} = \mathbf{r}_{ij}/r_{ij}$.

The potential of interaction between any two molecules i and j is

$$\mathfrak{U}_{ij}(ij) = \Phi_{ij}^{cc}(ij) + \Phi_{Ab}^{ss}(ij) \tag{3}$$

where $\Phi_{ij}^{cc}(ij)$ is the center-to-center potential and $\Phi_{AB}^{ss}(ij)$ is the potential between sites $[i, A]$ and $[j, B]$.

The electrostatic potential energy between two proteins in an ionic solution, which satisfies the Poisson-Boltzmann equation, may be expanded in an electrostatic multipole representation (Sheu et al., 1985). Since the terms higher than dipole in order are negligible, the expansion may be truncated at dipole order. The center-to-center interaction then is

$$\beta\Phi_{ij}^{cc}(ij) = U_{00,ij}(ij) + U_{11,ij}(ij) + U_{10,ij}(ij) + U_{01,ij}(ij), \tag{4}$$

where the subscripts 0 and 1 refer, respectively, to the coulombic and dipole contribution for each particle.

The orientation of $\mathbf{r}_{ij}$ with respect to a space-centered coordinate system is Ω_{ij}. The relative orientations of the molecules and center-to-center vector are given by the S functions (Rodger et al., 1992) as

$$S_{\ell_i\ell_j\ell}^{k_ik_j} = \sum_{m_im_jm} D_{m_ik_i}^{\ell_i}(\Omega_i) D_{m_jk_j}^{\ell_j}(\Omega_j) D_{m0}^{j}(\Omega_{ij}) \cdot \begin{pmatrix} \ell_i & \ell_j & j \\ m_i & m_j & m \end{pmatrix}, \tag{5}$$

where $D_{m_ik_i}^{l_i}$ is the Wigner rotation matrix, and the quantity in parenthesis is the Wigner $3-j$ symbol (Edmonds, 1960). The vector expansion functions (Stone, 1978)

$$\mathbf{V}_{\ell_i\ell_j:\lambda}^{k_ik_j} = \sum_{m_im_jm} i^{\ell_i-\ell_j-\lambda+1} D_{m_ik_i}^{\ell_i}(\Omega_i) D_{m_jk_j}^{\ell_j}(\Omega_j) C_{j\lambda1}^{m}(\Omega_{ij}) \cdot \begin{pmatrix} \ell_i & \ell_j & j \\ m_i & m_j & m \end{pmatrix} \tag{6}$$

are used in representing the central forces. In Eq. 6 $C_{j\lambda1}^{m}(\Omega_{ij})$ is the vector spherical harmonic (Stone, 1978).

In writing the expressions for the screened coulombic and dipole interactions, it is useful to write the Bjerrum length as

$$\mathfrak{B} = (e^-)^2\beta/[4\pi\epsilon_0\epsilon_{H_2O}]. \tag{7}$$

The charge on an electron is e^-, the permittivity of free space is $4\pi\epsilon_0$, and the dielectric constant of water is ϵ_{H_2O}. Let the charge on each counterion, with bulk concentration $\bar{n}_{o,\ell}$, be z_ℓ. The inverse Debye screening length is written

$$\kappa_D = \left[\mathfrak{B} \sum_\ell \bar{n}_{o,\ell} z_\ell^2 \right]^{1/2}. \tag{8}$$

The contact distance between particles i and j is defined to be $\sigma_{ij} = 1/2(\sigma_i + \sigma_j)$ and $a_i = \sigma_i/2$. We use twice the protein hydrodynamic radius (as determined from dynamic light scattering at 90° scattering angle, 17.5°C, in 0.15 $\mathfrak{M}$ PBSA, and 950 n $\mathfrak{M}$ protein concentration) as the particle diameter, σ_i. For convenience in writing the center-to-center potential model, let

$$p_{i,0} = Z_i\,\mathfrak{B}^{1/2}/\{1 + \kappa_D a_i\} \tag{9}$$

$$p_{i,1} = \{\mu_i\,\mathfrak{B}^{1/2}/e^-\}\left[2\left\{1 + \kappa_D a_i + \frac{(\kappa_D a_i)^2}{2}\right\} + \{1 + \kappa_D a_i\}\epsilon_i/\epsilon_{H_2O}\right]^{-1}. \tag{10}$$

The Yukawa screening parameter may be written as

$$E_{\ell_i\ell_j} = p_{i,\ell_i} p_{j,\ell_j} \exp(-\kappa_D\{r_{ij} - \sigma_{ij}\}) \tag{11}$$

where ℓ_i and ℓ_j take the values 0 and 1, respectively, for the charge and dipole contributions to the total potential energy. For compactness in the following discussion, define

$$q^{(1)}(ij) = 1 + \kappa_D r_{ij} + (\kappa_D r_{ij})^2/3 \tag{12}$$

$$q^{(2)}(ij) = 1 + \kappa_D r_{ij}. \tag{13}$$

The coulombic term for the center-to-center potential is

$$U_{00,ij}(ij) = E_{00}/r_{ij} \tag{14}$$

with central force, $\underline{F}_{00,ij}(ij) = -\bar{\nabla}_{r_j} U_{00,jj}(ij)$,

$$\underline{F}_{00,ij}(ij) = \frac{-\sqrt{3}\,E_{00}}{r_{ij}^2} q^{(2)}(ij)\mathbf{V}_{000:1}^{00}. \tag{15}$$

When the dipole is on particle i, then the dipole–charge potential of interaction is

$$U_{10,ij}(ij) = -\sqrt{3}\,\frac{E_{10}}{r_{ij}^2} q^{(2)}(ij) S_{101}^{00} \tag{16}$$

with force

$$\underline{F}_{10,ij}(ij) = -\frac{\sqrt{3}E_{10}}{r_{ij}^3}\cdot\{3q^{(1)}(ij)S_{101}^{00}\mathbf{V}_{000:1}^{00} + q^{(2)}(ij)\mathbf{V}_{101:0}^{00}\}. \tag{17}$$

Also,

$$U_{01,ij}(ij) = \sqrt{3}\frac{E_{01}}{r_{ij}^2}q^{(2)}(ij)S_{011}^{00} \tag{18}$$

with force

$$\underline{F}_{01,ij}(ij) = \frac{-\sqrt{3}E_{01}}{r_{ij}^3}\{3q^{(1)}(ij)S_{011}^{00}\mathbf{V}_{000:1}^{00} + q^{(2)}(ij)\mathbf{V}_{011:0}^{00}\}. \tag{19}$$

Finally, the dipole–dipole potential is

$$U_{11,ij}(ij) = -\sqrt{3}\frac{E_{11}}{r_{ij}^3}\{q^{(2)}(ij)S_{110}^{00} - 3\sqrt{3}q^{(1)}(ij)S_{101}^{00}S_{011}^{00}\} \tag{20}$$

and force

$$\underline{F}_{11,ij}(ij) = 9\frac{E_{11}}{r_{ij}^4}\cdot\left[\begin{array}{l} q^{(1)}(ij)[S_{011}^{00}\mathbf{V}_{101:0}^{00} + (S_{101}^{00}\mathbf{V}_{011:0}^{00} + S_{110}^{00}\mathbf{V}_{000:1}^{00})] \\ +5\left[q^{(2)}(ij) + \dfrac{2(\kappa_D r_{ij})^2}{5} + \dfrac{(\kappa_D r_{ij})^3}{15}\right]S_{101}^{00}S_{011}^{00} \end{array}\right]. \tag{21}$$

As discussed in the "Model Development" section, the epitope–paratope interaction depends upon intermolecular separation as well as mutual orientation of BSA and the antibody. The potential between $[i, A]$ and $[j, B]$ is modeled as a modified square well with respect to particle separation and square well with respect to mutual particle orientation. Specifically, the truncated cone model (Busch et al., 1994) is used for the paratope–epitope interaction. The apical angle of the cone representing $[i, A]$ is θ_A. The angle between $\mathbf{r}_{ij}$ and $\mathbf{r}_{is}$ is θ_i, while the angle between $\mathbf{r}_{ji}$ and $\mathbf{r}_{js}$ is θ_i. The step function

$$s(\theta_i, \theta_A) = \begin{cases} 1 & \text{for } \theta_i \le \theta_A \\ 0 & \text{for } \theta_i > \theta_A \end{cases} \tag{22}$$

describes the orientational dependence of the site-to-site potential. The separation dependence of the site-to-site potential is defined by $r_- < \sigma_{ij}$, $r_+ > \sigma_{ij}$ and $r_- < r_* < r_+$. The outer radius of the square well and inner radius of the triangular regions of the modified square well potential is r_*. The site-to-site potential is given by

$$\Phi_{AB}^{ss}(ij) = -s(\theta_i, \theta_A)s(\theta_j, \theta_B)\epsilon_{AB}\begin{cases} 1 & \text{for } r_- \le r_{ij} < r_* \\ (r_+ - r_{ij})/(r_+ - r_*) & \text{for } r_* \le r_{ij} \le r_+ \\ 0 & \text{otherwise.} \end{cases} \tag{23}$$

The values of the quantities for Eq. 23 are presented in the "Results" section.

Simulation Method

The association-biased Monte Carlo (ABMC) algorithm (Busch et al., 1994) was used to simulate the single-antigen, single-antibody system using 256 particles and a nominal pair potential cutoff of 30σ, $\sigma = \sum_i X^{(i)}\sigma_i$. The results of our Monte Carlo simulation, for the simple Yukawa potential with $\epsilon_{AB} = 0$, was in good agreement with published simulation results (Härtl et al., 1983; Härtl and Versold, 1988). We examined the effect of the number of equilibration cycles upon computed thermodynamic quantities and found no statistical difference when zero or 1.0×10^6 moves were used. Statistics were accumulated over 25,000 Monte Carlo particle move cycles.

Results

The parameters required for the model are the effective protein charge; net dipole moment with respect to the protein center of mass; the binding-site area; and energy of interaction. These parameters cannot be obtained in a straightforward simple manner for the following reasons. First, the binding-site area and energy cannot be determined independently of the protein center-to-center interaction. Second, the protein charge and dipole moment are either not available elsewhere in the literature or have been poorly determined for the proteins in this study. Third, the site areas and energies have not been previously determined for the proteins of interest. Therefore, we have had to obtain the values of some of the parameters by direct measurement (such as protein charge) and some of the others by estimate. The strategy used here is to first determine the net charge and dipole moment for each protein, then estimate the binding-site areas and potential energies from available experimental data.

The center-to-center potential given in Eq. 4 requires the effective diameter, surface charge of each protein, and dipole moment magnitude and direction. These quantities are summarized in Table 1 for the proteins used in this investigation. The hydrodynamic radius of BSA was determined from light-scattering measurements (90° scattering angle in 0.15 M PBS-A, 950-n M protein concentration and 17.5°C) to be 35.0 Å. The net effective charge on BSA at pH 7.2 was determined by titration (Tanford et al., 1955) to be $-16e^-$. The dipole moment for BSA has been experimentally measured to be 384.0 Debye units (D) (Soetewey et al., 1972). The static structure function for BSA, at 950-n M protein concentration, was not statistically different from unity for the range of the light-scattering wave numbers studied. This result was also obtained from the Monte Carlo simulation of BSA using the net protein charge of $-16.0e^-$ and dipole moment 384.0 D as specified in Table 1.

Table 1. Protein and Binding-Site Characteristics for BSA and anti-BSA Antibodies $Ab_{5.1}$, $Ab_{6.1}$, $Ab_{9.1}$

Parameter	BSA	$Ab_{5.1}$	$Ab_{6.1}$	$Ab_{9.1}$
Diameter (Å)	70.0±0.4	114.0±0.5	114.0±0.5	114.0±0.5
Isoelectric point	4.9–5.1	8.9–9.1	7.6–7.7	6.9–7.1
Charge (pH 7.2)	−16.0±0.4	36.0±1.0	10.0±0.8	5.0±2.0
Dipole Moment (debye)	384.0	445.0	445.0	445.0
Site Area (Å^2)	650.0	650.0	650.0	650.0
Site Energy ($/k_BT$)±0.005	—	0.700	1.357	2.244
Site Location	—	I-C	I-N	III-C
pK_A ABMC	—	7.84	8.41	7.81
pK_A Langmuir	—	7.84	8.42	7.80

The hydrodynamic radius of the three antibodies at the same conditions used for BSA is 54.0 Å. The net charge on each antibody was determined by titration measurements. The uncertainty on the charge of $Ab_{9.1}$ is due in part to the difficulty of determining the net charge on a protein near its isoelectric point in unbuffered solution. The charge of 5 on $Ab_{9.1}$ is certainly reasonable at pH 7.2 due to the range of the isoelectric point.

The dipole moment for each anti-BSA antibody is not known. The antiphosphorylcholine antibody MOPC21 (Adetugbo et al., 1977) is type IgG1, $\gamma 1$, and the amino acid sequence is known. The isoelectric point and computed net charge of MOPC21 are equivalent to our $Ab_{9.1}$. Since IgG1 antibodies have highly conserved amino acid sequences, except for the paratope region, we can use the MOPC21 charge distribution, excluding the antibody binding-site region, to represent the charge distribution in the antibodies used in this study. The charge vs. pH profile for the F_{ab} and F_c units of MOPC21 were estimated using the sequence analysis software package GCG (Version 6.0, Genetics Computer Group, Madison, WI). The net dipole moment is readily computed based upon the charges and centers of mass for each F_{ab} unit and the F_c unit of the antibody to be 2,607.7 D. Since the BSA has been characterized with respect to charge distribution (Peters, 1985) and dipole moment (Soetewey et al., 1972), we used the sequence analysis software package GCG and to obtain a net dipole moment of 2,254 D; a value that is 5.9 times higher than that determined by direct experimental measurements. The net measured dipole moment of a protein in solution will depend upon the polarizability of the protein, the screening of buried charges by the protein, screening of surface charges by water, and counter-ions. Since these factors are approximately independent of the type of protein, we scaled our raw estimate of the antibody dipole moment by 5.9 to obtain the quantities given in Table 1. Analysis of the amino acid sequence of the F_c unit of type MOPC21 antibodies shows that it is negatively charged at pH 7.2 while the F_{ab} units are positively charged. The dipole moment is then defined to be oriented from the carboxyl terminus of the antibody, labeled C in Figure 1, and bisects the hinge region between the two F_{ab} units. The dipole moment magnitudes of $Ab_{5.1}$ and $Ab_{6.1}$ are constrained to be equal to that of $Ab_{9.1}$ as we are immediately interested in charge interactions. With the center-to-center interaction characterized, we move on to characterizing the site-to-site interaction.

The approximate location of the epitopes to which $Ab_{5.1}$, $Ab_{6.1}$, and $Ab_{9.1}$ bind on BSA are shown in panel (a) of Figure 1. The surface areas of each epitope and paratope are not known. A survey of published X-ray crystallographic structures for antigen $-F_{ab}$ units indicated that the contact area varies from ~160 to ~900 Å^2, depending upon the antigen and type of antibody. The surface area was constrained to be equivalent to that for the antilysozyme antibody D1.3 (Bentley et al., 1989).

The antibody and antigen experience some mutual overlap upon binding. However, complete overlap will not occur due to electrostatic and hard core repulsion. The lower limit of particle separation for bond formation is set to be equal to the separation to which the pair distribution function for the nonassociating ($\epsilon_{AB} = 0$) system falls below 0.01. Specifically r_- is set to $0.898\sigma_{ij}$. Since the particle separation over which the epitope–paratope binding energy acts is $\sim O(10$ Å) (Wilder et al., 1975a,b), the outer diameter of the site, r_+, is set to be 10 Å beyond the particle contact distance. The binding site for each antigen–antibody pair is then a truncated cone, $c_t[i]$, bounded by concentric spheres of radius r_- and r_+ with apical angle, θ_A, such that the area of $c_t[i]$ intersecting the sphere of radius $\sigma_{ij}/2$ is 650 Å^2.

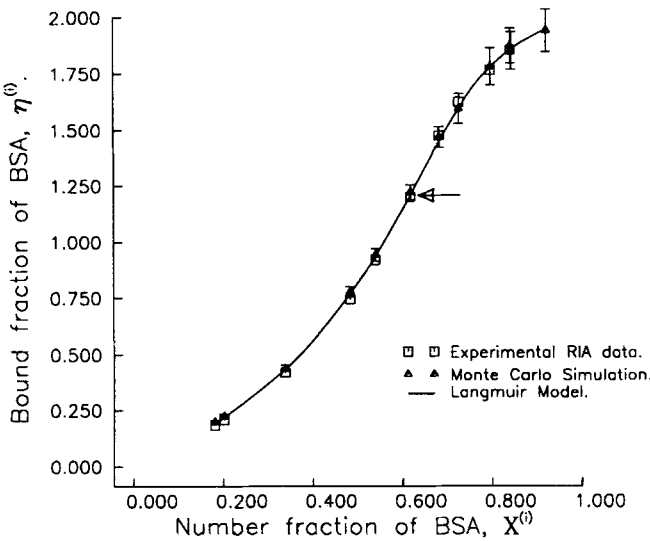

Figure 4. Equilibrium association graph for $Ab_{5.1}$ and BSA.

The graphs are normalized bound BSA, $\eta^{(i)} = [BSA]_B / [Ab_{5.1}]_T = (1 - q_0^{(i)})X^{(i)}/X^{(j)}$ vs. the total number fraction of BSA, $X^{(i)}$. The binding energy is 0.700 k_BT. The experimental data were obtained by radioimmunoassay (RIA) (Murphy et al., 1990).

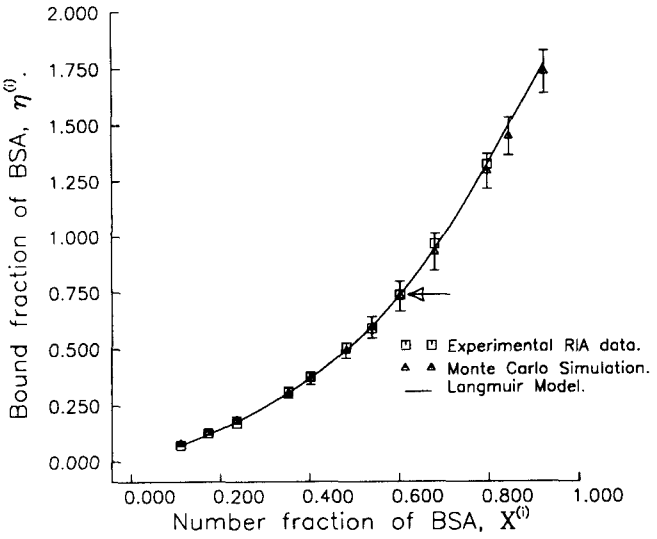

Figure 5. Equilibrium association graph for $Ab_{6.1}$ and BSA.

The graphs are normalized bound BSA, $\eta^{(i)} = [BSA]_B / [Ab_{6.1}]_T = (1 - q_0^{(i)})X^{(i)}/X^{(j)}$ vs. the total number fraction of BSA, $X^{(i)}$. The binding energy is 1.357 k_BT.

With the protein electrostatics, binding site location, and areas defined in the theoretical model, we estimated the energy of attraction for each BSA–antibody pair. The site energy, ϵ_{AB} in Eq. 23, was adjusted such that a match was found between the measured RIA and Monte Carlo-computed bound BSA fraction at a single total BSA number fraction. The point used for each BSA–antibody pair is marked with an arrow in Figures 4–6. In Table 1 the binding energy computed for each BSA–antibody pair is reported.

The bound fraction of BSA computed by Monte Carlo simulation ($\eta^{(i)} = (1 - q_0^{(i)})X^{(i)}/X^{(j)}$ and $q_0^{(i)}$ is the fraction of monomeric BSA in the equilibrium solution of BSA and antibody) is plotted with the measured values (Murphy et al., 1990) in Figure 4 for $Ab_{5.1}$ + BSA, Figure 5 for $Ab_{6.1}$ + BSA, and Figure 6 for $Ab_{9.1}$ + BSA. The agreement between the Monte Carlo-generated and experimental equilibrium binding graphs is quite good.

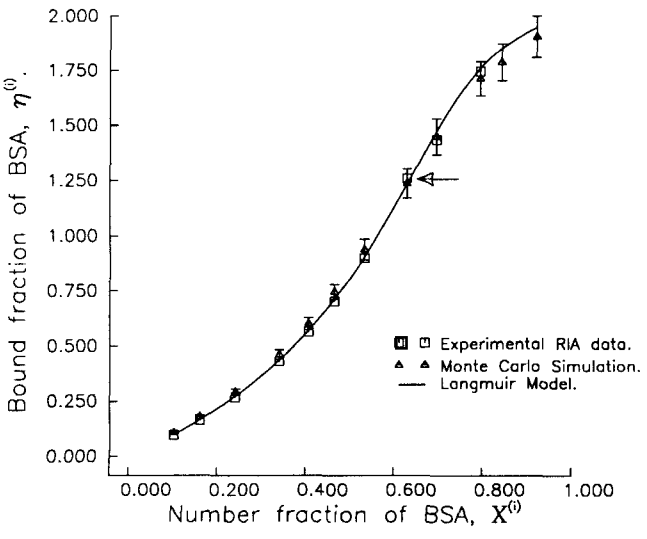

Figure 6. Equilibrium association graph for $Ab_{9.1}$ and BSA.

The graphs are normalized bound BSA, $\eta^{(i)} = [BSA]_B / [Ab_{9.1}]_T = (1 - q_0^{(i)})X^{(i)}/X^{(j)}$, vs. total number fraction of BSA, $X^{(i)}$. The binding energy is 2.244 k_BT.

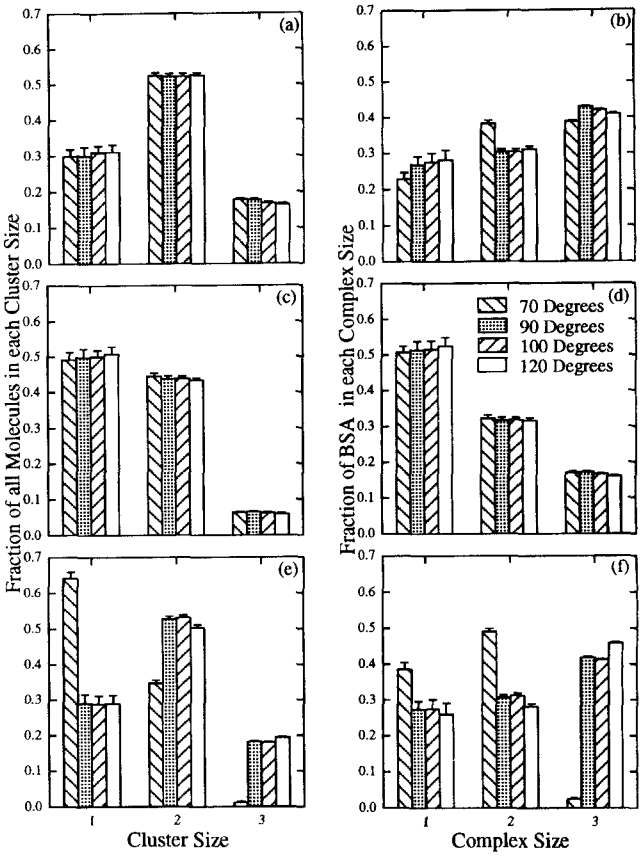

Figure 7. Monte-Carlo-generated cluster and complex size distribution for the BSA–antibody system.

The cluster distributions are given for $Ab_{5.1}$ + BSA in panel (a); $Ab_{6.1}$ + BSA in panel (c); $Ab_{9.1}$ + BSA in panel (e). The corresponding complex distributions are given in panels (b), (d), and (f). The histograms are given as a function of the angle between the paratopes, Ψ_{Ab}, on the antibody. The reduced densities and BSA number fractions are $Ab_{5.1}$ + BSA, $\rho^* = 2.0635 \times 10^{-5}$, $X^{(i)} = 158/256$; $Ab_{6.1}$ + BSA, $\rho^* = 2.0265 \times 10^{-5}$, $X^{(i)} = 153/256$; $Ab_{9.1}$ + BSA, $\rho^* = 2.0915$ x10^{-5}, $X^{(i)} = 161/256$. These quantities represent the experimental data indicated by arrows in Figures 4–6.

The angle between the paratopes was fixed to be 100° of arc for determination of the site-to-site binding energy. To investigate the influence of this angle, Ψ_{Ab}, upon the cluster and complex size distribution we simulated the equilibrium binding curve using $\Psi_{Ab} = [70, 90, 100, 120]$. We define a complex as a structure that includes only particles that are bound; that is, their relative orientation and separation satisfy Eq. 23. A cluster is composed of particles that are sufficiently close to form a bond but are not correctly oriented. The cluster and complex distributions for select state points and for each BSA–antibody pair are given in Figure 7. Specifically, the cluster and complex size distributions for

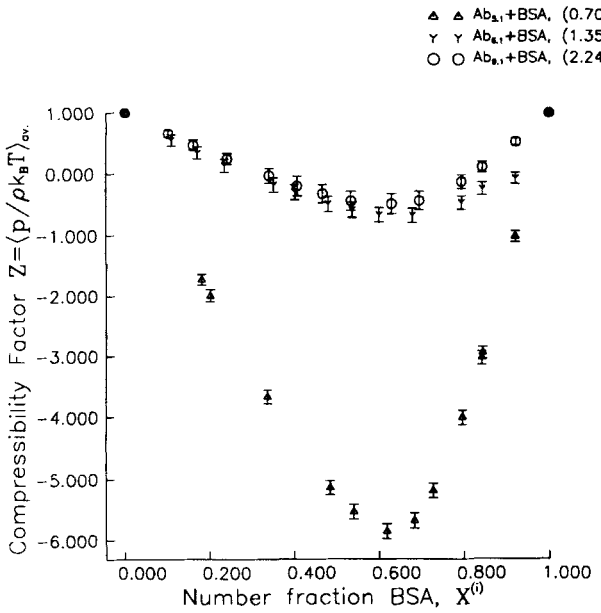

Figure 8. Compressibility factor, $\mathcal{Z}$ for the three systems, $Ab_{5.1}$+BSA, $Ab_{6.1}$+BSA, $Ab_{9.1}$+BSA in 0.15 $\mathfrak{M}$ PBS-A, 25.0°C computed by ABMC simulation.

The compressibility factor is plotted for each of the three antibody-BSA systems as a function of total number fraction of BSA, $X^{(i)}$.

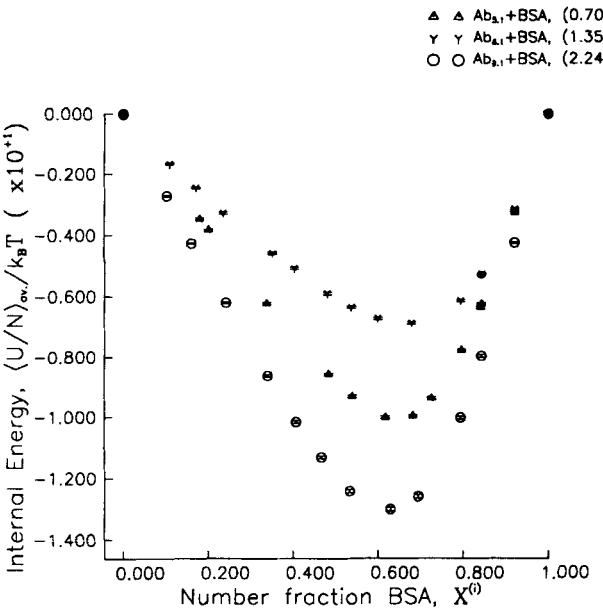

Figure 9. Total internal potential energy, $\mathfrak{U} = \langle U/N \rangle_{av}/k_BT$, for the three systems, $Ab_{5.1}$+BSA, $Ab_{6.1}$+BSA, $Ab_{9.1}$+BSA in 0.15 $\mathfrak{M}$ PBS-A, 25.0°C computed by ABMC simulation.

The total internal potential energy is plotted for each of the three antibody-BSA systems as a function of total number fraction of BSA, $X^{(i)}$.

$Ab_{5.1}$ + BSA at $\rho^* = 2.0635 \times 10^{-5}$, $X^{(i)} = 158/256$ are given in panels (a) and (b); $Ab_{6.1}$ + BSA at $\rho^* = 2.0265 \times 10^{-5}$, $X^{(i)} = 153/256$ are given in (c) and (d); $Ab_{9.1}$ + BSA at $\rho^* = 2.0915 \times 10^{-5}$, $X^{(i)} = 161/256$ are given in panels (e) and (f). In all cases, the temperature is 25°C, the solvent is 0.15 $\mathfrak{M}$ PBSA. For each BSA–antibody pair study, the computed complex and cluster size distributions are independent of angle between the F_{ab} units for angles greater than 90° of arc.

Since the reduced number density of proteins in the BSA–antibody systems studied here is $O(1.0 \times 10^{-5})$, then the compressibility factor $\mathcal{Z}$ is approximately unity when $\epsilon_{AB} = 0$. Any deviation of $\mathcal{Z}$ from unity is due to protein association. The compressibility factor is plotted in Figure 8 for the three antibodies against BSA and as a function of total number fraction of BSA. The minimum in the compressibility factor vs. total number fraction of BSA occurs at the expected value of $X^{(i)} = 2/3$. The striking difference between the BSA–antibody pairs $Ab_{5.1}$ + BSA and $Ab_{6.1}$ + BSA, $Ab_{9.1}$ + BSA is due to the large charge on the $Ab_{5.1}$ molecule in comparison to $Ab_{6.1}$ and $Ab_{9.1}$.

The total internal potential energy includes both the center-to-center and site-to-site potential energy of interaction and is a function of the number of BSA–antibody bonds formed. The internal potential energy for the three antibodies against BSA ($Ab_{5.1}$ + BSA, $Ab_{6.1}$ + BSA, and $Ab_{5.1}$ + BSA), as a function of the total number fraction of BSA, $X^{(i)}$ is plotted in Figure 9. As with the compressibility factor, the internal potential energy exhibits a nonsymmetric minimum at $X^{(i)} = 2/3$. The smaller magnitudes of the internal potential energy obtained for $Ab_{6.1}$ + BSA reflects the smaller number of bonds formed in this system than are found for either $Ab_{5.1}$ + BSA or $Ab_{9.1}$ + BSA.

While illustrating the presence of an association between BSA and the antibody leading to a condensed state of the proteins in solution, the negative compressibility factor shown in Figure 8 lacks physical meaning. The use of osmotic pressure data permits physical interpretation of our Monte Carlo simulation results. Define the reduced second virial coefficient as $\mathfrak{B}_2^* = \mathfrak{B}_2/\sigma^3$. Since the solute density is quite low the total internal virial may be expressed as $\langle \mathcal{W} \rangle_{av} = \mathfrak{B}_2^* \rho^*$. For the system of proteins in solution with counterions the compressibility factor is proportional to the solution osmotic pressure. Write the osmotic pressure as an expansion truncated to first order in solute number density to obtain

$$\beta \frac{\Pi}{\rho_T} = 1 + \mathfrak{B}_2^* \rho^*. \tag{24}$$

The osmotic pressure and isothermal compressibility of the proteins in solution are directly related. The isothermal compressibility is, by definition, proportional to the static structure function at zero wave number. The static structure function may be obtained from dynamic light-scattering measurements; it may also be computed directly from Monte Carlo simulation results.

The osmotic pressure and static structure function at zero scattering angle, $\mathcal{S}(0)$, are related as

$$\beta \left(\frac{\partial \Pi}{\partial \rho} \right)_T = 1/\mathcal{S}(0). \tag{25}$$

Table 2. Comparison of Experimental and Simulation Thermodynamic Quantities for BSA and anti-BSA Antibodies

System	Simulation		Experimental	
	$\mathcal{B}_2^*$	$\mathcal{S}(0)$	$\mathcal{B}_2^*$	$\mathcal{S}(0)$
Reduced density $= 5.176\times10^{-4}$				
BSA	2.356	0.9975	1.399	0.9970
$Ab_{5.1}$	2.425	0.9971	—	~1.0
$Ab_{6.1}$	0.763	0.9982	—	~1.0
$Ab_{9.1}$	0.204	0.9982	—	~1.0
Reduced density $= 9.5933\times10^{-4}$				
PSA + $Ab_{5.1}$	−1.559	1.0029	—	—
PSA + $Ab_{6.1}$	1.568	0.9972	—	—
PSA + $Ab_{9.1}$	1.621	0.9969	—	—
BSA + $Ab_{5.1}$	−248.5	1.911	−195.0 ± 10.0	1.6 ± 0.05
BSA + $Ab_{6.1}$	−239.6	1.851	−180.0 ± 11.0	1.56 ± 0.07
BSA + $Ab_{9.1}$	−238.2	1.842	−175.0 ± 15.0	1.5 ± 0.07

Therefore

$$\beta^{-1}\left(\frac{\partial\rho^*}{\partial p}\right)_T = \rho^*\beta^{-1}\chi_T = \mathcal{S}(0) = 1 + \rho^*\int[g_T(r)-1]\,d^3r, \tag{26}$$

From Eqs. 24 and 26 we obtain that

$$\mathcal{B}_2^* = \frac{1-\mathcal{S}(0)}{2\,\mathcal{S}(0)\rho^*}. \tag{27}$$

Equation 27 provides a clear and simple connection between the zero wave-number static structure function, or isothermal compressibility, and the second virial coefficient, or the osmotic pressure. Equation 27 also provides a check on the consistency between experimental and Monte Carlo generated results.

The computed and experimental second virial coefficients and static structure function at zero wave number for several protein systems are presented in Table 2. The computed value of 2.356 for the second virial coefficient of BSA is within the experimental range of 1.40 (Shaw, 1976) and 3.10 (Scatchard et al., 1950). For the protein pairs $Ab_{5.1}$ + BSA, $Ab_{6.1}$ + BSA, and $Ab_{9.1}$ + BSA, Monte Carlo results given in Table 2 indicate values of $\mathcal{S}(0)$ that are statistically different from unity. The second virial coefficient for the pair $Ab_{5.1}$ + BSA is significantly less than for the pair $Ab_{9.1}$ + BSA. To examine this trend more carefully we replaced BSA in solution by its homologue porcine serum albumin (PSA). PSA has the same isoelectric point, molecular weight, and hydrodynamic radius as BSA. PSA, however, does not bind to the antibodies used in this study. The results for the PSA + anti-BSA antibody systems reported in Table 2 show that the second virial coefficient becomes increasingly negative with increasing PSA/anti-BSA antibody attraction. We conclude that the decrease in second virial coefficient between the $Ab_{9.1}$ + BSA and $Ab_{5.1}$ + BSA systems is due to the greater multipole attraction between BSA and $Ab_{5.1}$. The magnitude difference between the PSA + anti-BSA antibody and BSA + anti-BSA antibody systems is due to the association between BSA and the antibodies.

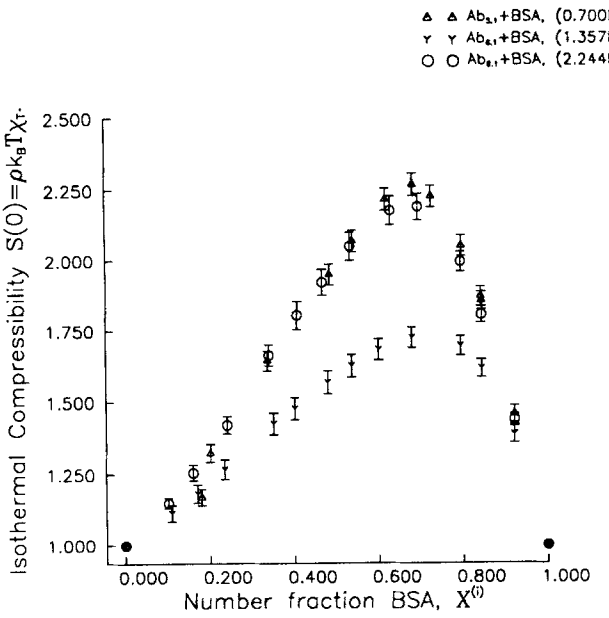

Figure 10. Normalized isothermal compressibility, $\rho k_B T\chi_T$, for the three systems, $Ab_{5.1}$+BSA, $Ab_{6.1}$+BSA, $Ab_{9.1}$+BSA in 0.15 M PBS-A, 25.0°C computed by ABMC simulation.

The static structure function at zero wave number, which is proportional to the isothermal compressibility, is plotted for each of the three antibody-BSA systems as a function of total number fraction of BSA, $X^{(i)}$.

Considering the normalized isothermal compressibility [we use $\mathcal{S}(0) = \rho k_B T\chi_T$ as the normalized isothermal compressibility] as a function of total BSA number fraction, we can study the influence of BSA–antibody binding upon the osmotic pressure. In Figure 10 we present the normalized isothermal compressibility for the three systems $Ab_{5.1}$ + BSA, $Ab_{6.1}$ + BSA, and $Ab_{9.1}$ + BSA. Association between BSA and the antibody has the effect of increasing the isothermal compressibility near epitope–paratope equivalence at $X^{(i)} = 2/3$. The isothermal compressibility for $Ab_{5.1}$ + BSA and $Ab_{9.1}$ + BSA, as a function of total BSA number fraction, are statistically the same; the system $Ab_{6.1}$ + BSA yields an isothermal compressibility that is less than both $Ab_{5.1}$ + BSA and $Ab_{9.1}$ + BSA for all $X^{(i)}$. Since $Ab_{5.1}$ and $Ab_{9.1}$ bind BSA with nearly the same affinity, then the isothermal compressibility is expected to be the same for these two systems, except for the electrostatic effects previously discussed. The affinity of $Ab_{6.1}$ is less than either $Ab_{5.1}$ or $Ab_{9.1}$ for BSA, hence the isothermal compressibility is lower than both $Ab_{5.1}$ and $Ab_{9.1}$.

Discussion

Analysis of antigen–antibody equilibrium binding data using the Langmuir isotherm is a common method for determining the number of active sites on the antibody and the affinity between the antigen and antibody. This method of analysis relies on a macroscopic description of the system and therefore does not reveal information on the underlying molecular physics of the interaction. Such a macroscopic description cannot be used to describe the influence of associa-

tion between particles of the system upon measurable thermodynamic properties.

Thermodynamic perturbation theory (TPT) (Wertheim, 1984), like the current method, yields the equilibrium binding data given a description of the association between molecules in the system. Once the model has been specified, TPT then yields the bound fraction, and Helmholtz free energy and potential energy change due to the association. However, an in-depth study of the efficacy of TPT in predicting the thermodynamic properties of real systems has, to our knowledge, not been conducted. The three main areas where TPT is known to be deficient are critical to our study of immune complex formation: First, TPT is unable to give the pair distribution outside the binding-site region; second, TPT is not sufficiently developed to accurately predict the behavior of associating particles where the angle between binding sites is different from π radians; third, TPT (or any other currently available analytic theory of associating fluids) is unable to yield structural information on the immune complexes. Our model was developed to overcome some of these limitations and to permit estimation of thermodynamic properties as a function of protein charge, dipole moment, and binding-site location.

An estimation of the second virial coefficient for the three BSA–antibody systems was possible because $\mathcal{S}_T(0)$ obtained from light scattering was statistically different from unity. Comparing the results for $Ab_{9.1}$ + BSA, $Ab_{6.1}$ + BSA, and $Ab_{5.1}$ + BSA (see Table 2), we observe that both the sign and magnitude agree with expectations for an increasingly attractive system. The difference in results between the PSA–antibody and BSA–antibody systems is due predominantly to the binding of BSA to the antibodies. If $Ab_{5.1}$, $Ab_{6.1}$, and $Ab_{9.1}$ were identical in charge and dipole moment orientation with respect to their respective epitopes, then we would expect that $\mathcal{S}(0)$ and subsequently $\mathcal{B}_2^*$ to be identical for the proteins in solution with BSA. The fact that $Ab_{5.1}$ is more cationic than $Ab_{9.1}$ and that the epitope for each antibody is oriented in vastly different locations with respect to the BSA dipole moment is reflected in both $\mathcal{S}(0)$ and $\mathcal{B}_2^*$. Our simulation results (data not shown) also indicate that the excluded volume is obtained for the reduced second virial coefficient of a single-protein system in the limit of zero for both the charge and dipole moment on the proteins. However, even in the limit of zero charge the reduced second virial coefficient is not necessarily zero due to the nonzero dipole–dipole interactions.

If the structural details of the paratope–epitope interaction were known, then the energy of interaction between the paratope and epitope could be determined, albeit model based. One would not expect that this particular energy would yield the experimental affinity constant. The experimental affinity constant includes solvation of each protein, entropic effects such as rearrangement of the solvent, ion, and counter ions, as well as energetic effect, including long-ranged charged group interaction and excluded volume. Thus the energy computed from close-range atom–atom proximity would be a rather poor estimate of the experimentally determined affinity constant.

A large number of site-to-site and center-to-center potential energy combinations, $(\Phi_{ij}^{cc}(ij), \Phi_{AB}^{ss}(ij))$, will reproduce the equilibrium binding graphs presented in Figure 4 for $Ab_{5.1}$ + BSA, Figure 5 for $Ab_{6.1}$ + BSA, and Figure 6 for $Ab_{9.1}$ + BSA. By comparing the site-to-site energy for the $Ab_{5.1}$ + BSA system ($\epsilon_{AB} = 0.70$) with the $Ab_{9.1}$ + BSA system ($\epsilon_{AB} = 2.244$), we conclude that the computed site-to-site energy is sensitive to the charge on the protein. Since the protein center-to-center potential is dependent upon the net surface charge and dipole, then only a single site-to-site potential for each protein pair will reproduce the equilibrium binding graphs. Altering the dipole moment direction, which reflects different possible charge distributions on the proteins, will affect the value for the site-to-site energy, but will not influence the overall agreement between computed and experimental equilibrium binding results. Hydrophobic interactions, and dehydration of contacting surfaces, require both water molecules and counterions in the simulation. If these were to be included the nature of the center-to-center potential, particularly at low separation, would be altered.

Estimating the charge distribution using that computed for the IgG1 $\gamma 1$ antibody MOPC21 may not provide an accurate picture for all IgG1 $\kappa 1$ antibodies. The charge distribution is used to determine the direction of the dipole moment on the antibody and provide a starting point for estimating its magnitude. An order of magnitude error in the charge distribution of the IgG1 antibodies will not change the direction of the dipole moment, since the direction depends only upon the signs of the net charge on the F_c and F_{ab} units. An order-of-magnitude error in estimating the charge distribution will, however, influence the magnitude of the dipole moment. However, the equilibrium binding graph computed by the Monte Carlo simulation will remain unchanged, since it depends upon the combined center-to-center and binding-site energies.

Finally, now that we have shown that our model is able to predict the available thermodynamic values a select set of BSA/anti-BSA antibody systems, we are in a position to study a system containing two antibodies with a single antigen. This particular system will form n-member complexes that can, under certain circumstances, form ring structures. By manipulating the center-to-center and site-to-site potential energies and the relative location of the epitopes on the surface of BSA, a more extensive investigation of the physical phenomena leading to observed immune complex distributions can be performed.

Acknowledgment

This work was supported by NIH grants CA-45272 and CA-01401. One of the authors (N.B.) was supported by a NIH predoctoral biotechnology fellowship (GM-08339) and a Johnson and Johnson fellowship. We also acknowledge the computer time generously provided by the Rutgers University Computer and the Michigan Technological University Computer Center.

Literature Cited

Ackerson, B. J., "Correlations for Interacting Particles," *J. Chem. Phys.*, **64**, 242 (1976).

Adetugbo, K., C. Milstein, and D. S. Secher, "Molecular Analysis of Spontaneous Somatic Mutants," *Nature*, **265**, 299 (1977).

Amit, A. G., R. A. Mariuzza, S. E. V. Phillips, and R. J. Poljak, "Three-Dimensional Structure of an Antigen–Antibody Complex at 2.8Å Resolution," *Science*, **233**, 747 (1986).

Bentley, G. A., T. N. Bhat, G. Boulot, T. Fischmann, J. Navaza, R. J. Poljak, M. M. Riottot, and D. Tello, "Immunochemical and Crys-

tallographic Studies of Antibody D1.3 in Its Free, Antigen-Liganded and Idiotope-Bound States," *Cold Spring Harbor Symp. Quantitative Biology*, **54**, 239 (1989).
Berne, B., and R. Pecora, *Dynamic Light Scattering*, Wiley, New York (1975).
Buckingham, A. D., and J. A. Popel, "The Statistical Mechanics of Imperfect Polar Gases: 1. Second Virial Coefficients," *Trans. Faraday Soc.*, **51**, 1173 (1955).
Buckingham, A. D., and J. A. Popel, "The Statistical Mechanics of Imperfect Polar Gases: 2. Dielectric Polarization," *Trans. Faraday Soc.*, **51**, 1179 (1955).
Busch, N. A., M. S. Wertheim, Y. C. Chiew, and M. L. Yarmush, "A Monte Carlo Method for Simulation Associating Fluids," *J. Chem. Phys.*, **101**(4), 3147 (1994).
Edmonds, A. R., *Angular Momentum in Quantum Mechanics*, Princeton Univ. Press, Princeton, NJ (1960).
Garred, P., T. E. Michaelsen, and A. Åse, "The IgG SubClass Pattern of Complement Activation Depends on Epitope Density and Antibody and Complement Concentration," *Scand. J. Immunol.*, **30**, 379 (1989).
Garred, P., T. E. Mullnes, L. Thorsteinsson, K. Erlendsson, and K. Steinsson, "Increased Amounts of C4 Containing Immune Complexes and Inefficient Activation of C3 and Terminal Complement Pathway in a Patient with Homozygous C2 Deficiency and Systemic Lupus Erythmeatosus," *Scand. J. Immunol.*, **31**, 59 (1990).
Härtl, W., and H. Versold, "Liquid-Like Ordered Colloidal Suspensions: The Influence of the Particle Concentration," *J. Chem. Phys.*, **88**, 7157 (1988).
Härtl, W., H. Versold, and U. Wittig, "Liquid Like Structure of Charged Colloidal Dispersions in the Presence of Screening Ions," *Mol. Phys.*, **50**, 815 (1983).
Morel, G., D. M. Yarmush, C. K. Colton, D. C. Benjamin, and M. L. Yarmush, "Monoclonal Antibodies to Bovine Serum Albumin: Affinity and Specificity Determinations," *Mol. Immunol.*, **25**, (1988).
Murphy, R. M., "Antigen-Antibody Complexes: Size, Conformation, and Reactivity with Protein A," PhD Thesis, MIT, Cambridge, MA (1989).
Murphy, R. M., R. A. Chamberlin, P. Schurtenberger, C. K. Colton, and M. L. Yarmush, "Size and Structure of Antigen-Antibody Complexes: Thermodynamic Parameters," *Biochem.*, **29**, 10889 (1990).
Murphy, R. M., J. Slayter, P. Schurtenberger, R. A. Chamberlin, C. K. Colton, and M. L. Yarmush, "Size and Structure of Antigen-Antibody Complexes: Electron Microscopic and Light Scattering Studies," *Biophys. J.*, **54**, 45 (1988).
Padlan, E. A., E. W. Silverton, S. Sheriff, G. H. Cohen, S. J. Smith-Gill, and D. R. Davies, "Structure of an Antibody-Antigen Complex: Crystal Structure of the HyHEL10 F_{ab}-lysozyme Complex," *Proc. U.S. Natl. Acad. Sci.*, **86**, 5939 (1990).
Paul, W. E., *Fundamental Immunology*, Raven Press, New York (1986).
Pauling, L., "A Theory of the Structure and Process for Formation of Antibodies," *J. Am. Chem. Soc.*, **62**, 2643 (1940).
Peters, T., "Serum Albumin," *Advances in Protein Chemistry*, Vol. 37, Academic Press, New York (1985).
Provencher, S. W., "Inverse Problems in Polymer Characterization: Direct Analysis of Polydispersity with Photon Correlation Spectroscopy," *Macromol. Chem.*, **180**, 201 (1979).
Rodger, P. M., A. J. Stone, and D. J. Tildesely, "Anisotropic Site-Site Potentials in Molecular Dynamics," *Mol. Simulation*, **8**, 145 (1992).
Scatchard, G., I. H. Scheinberg, and H. Armstrong, "Physical Chemistry of Protein Solutions: IV. The Combination of Human Serum Albumin With Chloride Ion," *J. Am. Chem. Soc.*, **72**, 535 (1950).
Segal, D. M., S. K. Dower, and J. A. Titus, "The FcR Mediated Endocytosis of Model Immune Complexes by Cells from the P3338D1 Mouse Macrophage Line," *J. Immunol.*, **130**, 130 (1983).
Shaw, M., "Interpretation of Osmotic Pressure in Solutions of One and Two Non-Diffusible Components," *Biophys. J.*, **16**, 43 (1976).
Sheu, E. Y., C.-F. Wu, S.-H. Chen, and L. Blum, "Application of a Rescaled Mean Spherical Approximation to Strongly Interacting Ionic Micellar Solutions," *Phys. Rev. A*, **32**, 3807 (1985).
Soetewey, F., M. Rosseneau-Motreff, R. Lamotte, and H. Peeters, "Size and Shape Determination of Native and Defatted Bovine Serum Albumin Monomers: II. Influence of the Fatty Acid Content on the Conformation of Bovine Serum Albumin Monomers," *J. Biochem.*, **71**, 705 (1972).
Stone, A. J., "The Description of Biomolecular Potentials, Forces and Torques: The **S** and **V** Function Expansions," *Mol. Phys.*, **36**, 241 (1978).
Tanford, C., "Hydrogen Ion Titration Curves of Proteins," *Proc. Iowa Academy of Science*, **59**, 206 (1952).
Tanford, C., "Hydrogen Ion Titration Curves of Proteins," *Electrochemistry in Biology and Medicine* (1955).
Tanford, C., S. A. Swanson, and W. S. Shore, "Hydrogen Ion Equilibria of Bovine Serum Albumin," *J. Am. Chem. Soc.*, **77**, 6414 (1955).
Tulip, W. R., J. N. Varghese, R. G. Webster, G. M. Air, W. G. Laver, and P. M. Colman, "Crystal Structures of Neuraminidase-Antibody Complexes," *Cold Spring Harbor Symp. Quantitative Biology*, **54**, 257 (1989).
Weiss, L., F. Maillet, and M. Kaxatchkine, "Lupus and Protein Deficiencies of the Classical Complement Pathway," *Rev. Prat.*, **21**(21), 1937 (1990).
Wertheim, M. S., "Fluids with Highly Directional Attractive Forces: I. Statistical Thermodynamics," *J. Stat. Phys.*, **35**(1), 19 (1984).
Wilder, R. L., G. Green, and V. Schumaker, "Bivalent Hapten-Antibody Interactions: 2. Bivalent Haptens as Probes of Combining Site Depth," *Immunochem.*, **12**, 49 (1975a).
Wilder, R. L., G. Green, and V. Schumaker, "Bivalent Hapten-Antibody Interactions. I. A Comparison of Water Soluble and Water Insoluble Bivalent Haptens," *Immunochem.*, **12**, 39 (1975).

Manuscript received June 8, 1994, and revision received Nov. 22, 1994.